

# Effect of Ce Doping on Structural and Magnetical Properties of $(\text{Sm}_{1-y}\text{Ce}_y)_2\text{Fe}_{17}\text{N}_x$

Xu Jianwei<sup>1</sup>, Zheng Jingwu<sup>1</sup>, Chen Haibo<sup>2</sup>, Qiao Liang<sup>1</sup>, Ying Yao<sup>1</sup>, Cai Wei<sup>1</sup>,  
Li Wangchang<sup>1</sup>, Yu Jing<sup>1</sup>, Lin Min<sup>3</sup>, Che Shenglei<sup>1</sup>

<sup>1</sup> Zhejiang University of Technology, Hangzhou 310014, China; <sup>2</sup> Hangzhou Haisheng Technology Co., Ltd, Hangzhou 310019, China;

<sup>3</sup> Ningbo Institute of Material Technology & Engineering, Chinese Academy of Sciences, Ningbo 315201, China

**Abstract:** Magnetic properties and microstructure of fully nitrated  $(\text{Sm}_{1-y}\text{Ce}_y)_2\text{Fe}_{17}\text{N}_x$  ( $y = 0, 0.20, 0.33, 0.45, 0.50, 0.67, 0.80, 1.00$ ) powders have been investigated. When 33 at% Ce is substituted for Sm, maximum energy product  $(BH)_{\max}$  changes from 141.6  $\text{kJ/m}^3$  to 140.1  $\text{kJ/m}^3$  with almost no decrease. Accordingly, performance/rare earth price ratio increases by 39.6%. According to the energy dispersive spectroscopy (EDS) analysis, Ce tends to be distributed in the  $\text{REFe}_3/\text{REFe}_2$  grain boundary phase. Meanwhile, valence change of the Ce ion in  $(\text{Sm}_{1-y}\text{Ce}_y)_2\text{Fe}_{17}\text{N}_x$  was confirmed by XPS.

**Key words:**  $\text{Sm}_2\text{Fe}_{17}\text{N}_x$ ; Ce substitution; maximum energy product; phase aggregation; Ce valence shift

Bonded permanent magnets (bonded PMs) have extremely low eddy current loss due to their low electrical conductivity<sup>[1,2]</sup>. Therefore, in a high-speed motor using PMs of the same weight, the bonded PMs can better suppress the reduction of the output power of the motor compared with the sintered PMs<sup>[1,2]</sup>. The corresponding motor has a higher efficiency<sup>[1,2]</sup>.  $\text{Sm}_2\text{Fe}_{17}\text{N}_x$  has high magnetic properties comparable to  $\text{NdFeB}$ <sup>[3-9]</sup>, including high saturation magnetization ( $M_s=162.9 \text{ A}\cdot\text{m}^2/\text{kg}$ ), strong uniaxial anisotropy field ( $H_A=26 \text{ T}$ ) and high Curie temperature ( $T_C=473 \text{ }^\circ\text{C}$ ). Although the initial degradation temperature of about  $600 \text{ }^\circ\text{C}$  hinders the use of  $\text{Sm}_2\text{Fe}_{17}\text{N}_x$  as sintered PMs<sup>[10]</sup>, the above high magnetic properties still make  $\text{Sm}_2\text{Fe}_{17}\text{N}_x$  powder suitable for bonded PMs<sup>[10,11]</sup>. Anisotropic  $\text{Sm}_2\text{Fe}_{17}\text{N}_x$  PMs are expected to share the anisotropic rare earth (RE) bonded PM market with HDDR anisotropic Nd-Fe-B PMs<sup>[12,13]</sup>.

Since samarium (Sm) accounts for only 3.2% of RE in the earth's crust<sup>[14]</sup>, the shortage of Sm will become a problem once  $\text{Sm}_2\text{Fe}_{17}\text{N}_x$  is used on a large scale. Cerium (Ce) is the most abundant RE, accounting for up to 30.2% of RE in the earth's crust<sup>[14]</sup>. At the same time, due to the unbalanced use of

RE, a large amount of Ce is not used and is idle<sup>[14,15]</sup>. It is of great value to replace Sm with Ce in  $\text{Sm}_2\text{Fe}_{17}\text{N}_x$  PM.

Some studies have been conducted on Ce-doped  $\text{Sm}_2\text{Fe}_{17}\text{N}_x$ <sup>[16-18]</sup>. The experiment of Huang et al<sup>[16]</sup> showed that as the Ce content increased,  $M_s$  of  $(\text{Sm}_{1-y}\text{Ce}_y)_2\text{Fe}_{17}\text{N}_x$  increased and  $H_A$  decreased. Subsequently, it was verified by Tribhuvan Pandey et al<sup>[17]</sup> with the first-principles calculations. Unfortunately, the variation of magnetic properties such as  $(BH)_{\max}$ ,  $B_r$  and  $H_{cJ}$  of  $(\text{Sm}_{1-y}\text{Ce}_y)_2\text{Fe}_{17}\text{N}_x$  with Ce addition has not been reported.  $(BH)_{\max}$  is an important indicator of permanent magnet materials, and its theoretical maximum is related to  $\frac{(\mu_0 M_s)^2}{4}$ .

As described above, with Ce content increasing,  $M_s$  of  $(\text{Sm}_{1-y}\text{Ce}_y)_2\text{Fe}_{17}\text{N}_x$  increases. Therefore, is it possible to improve  $(BH)_{\max}$  of  $(\text{Sm}_{1-y}\text{Ce}_y)_2\text{Fe}_{17}\text{N}_x$  by replacing Sm with an appropriate amount of Ce? The question is answered through experiments in this article. In addition, Huang et al<sup>[16]</sup> and Chin et al<sup>[18]</sup> speculated that there was a possibility of valence shift of the Ce ion in  $(\text{Sm}_{1-y}\text{Ce}_y)_2\text{Fe}_{17}\text{N}_x$ . This paper verified the hypothesis by experiment.

Received date: October 11, 2019

Foundation item: State Key Laboratory of Rare Earth Permanent Magnetic Materials Opening Foundation (SKLREPM17OF06); National Natural Science Foundation of China (U1802254, 51871201); Xinmiao Talent Planning of Zhejiang Province (2019R403055)

Corresponding author: Che Shenglei, Ph. D., Professor, College of Materials Science and Engineering, Zhejiang University of Technology, Hangzhou 310014, P. R. China, Tel: 0086-571-88320450, E-mail: cheshenglei@zjut.edu.cn

Copyright © 2020, Northwest Institute for Nonferrous Metal Research. Published by Science Press. All rights reserved.

### 1 Experiment

The precursor ingots with nominal composition of  $(\text{Sm}_{1-y}\text{Ce}_y)_2\text{Fe}_{17}$  were prepared by arc melting constituent metals in an argon atmosphere, and  $y$  (atomic fraction of Ce) varies from 0 to 1.00 ( $y = 0, 0.20, 0.33, 0.45, 0.50, 0.67, 0.80, 1.00$ ). A 35 wt% excess of Sm was added to compensate for losses due to evaporation. Each ingot was remelted four times and annealed at 1200 °C for 12 h to ensure uniform composition. The samples were heated in a hydrogen atmosphere at 300 °C for 2 h, and cracks formed along the grain boundaries<sup>[19]</sup>. Subsequently, the samples were nitrided in a  $\text{NH}_3\text{-H}_2$  (1:2 vol/vol) atmosphere<sup>[20]</sup> at 440 °C for 6 h, and then annealed at 470 °C for 3 h in an argon atmosphere to remove the adsorbed hydrogen<sup>[21]</sup>. Then, the ingots were ground into powder and the powder was sieved through a 74  $\mu\text{m}$  in hole diameter sieve. This was followed by ball milling. The ball milling was carried out in a stainless- steel vial and isopropanol was used as a carrier liquid. The agate balls used for grinding had a diameter of 4 mm. The ball to powder weight ratio was 20:1. The ball mill was carried out at 300 r/min for 2 h on a horizontal planetary ball mill (Nanjing NanDa Instrument Plant /QM-WX4). After drying,  $(\text{Sm}_{1-y}\text{Ce}_y)_2\text{Fe}_{17}\text{N}_x$  powder was obtained.

The  $(\text{Sm}_{1-y}\text{Ce}_y)_2\text{Fe}_{17}\text{N}_x$  powder was mixed with an epoxy resin and then aligned in a magnetic field of 2.8 T until the mixed resin was cured. The magnetization measurements were

performed in a physical performance measurement system (PPMS, Quantum Design/PPMS-9), with a maximum field of 7 T (the density of the  $(\text{Sm}_{1-y}\text{Ce}_y)_2\text{Fe}_{17}\text{N}_x$  powder used to calculate the saturation magnetization was 7.67  $\text{g}/\text{cm}^3$  [22]).  $H_A$  of  $(\text{Sm}_{1-y}\text{Ce}_y)_2\text{Fe}_{17}\text{N}_x$  powder at 25 and 100 °C was obtained by measuring the magnetization parallel to and perpendicular to the alignment direction on powder which was aligned in the epoxy resin. The phase composition of the nitrided powder was analyzed by X-ray diffraction (XRD, PANalytical/X'Pert Pro) with Cu  $K\alpha$  radiation. The microstructure of the  $(\text{Sm}_{1-y}\text{Ce}_y)_2\text{Fe}_{17}\text{N}_x$  powder was investigated by scanning electron microscopy (SEM, Hitachi/SU1510). The cross-section chemical composition of the unnitrided  $(\text{Sm}_{1-y}\text{Ce}_y)_2\text{Fe}_{17}$  alloy was analyzed using a field emission scanning electron microscope (FESEM, FEI Nova Nano SEM 450) equipped with a backscattered electron (BSE) probe and an energy-dispersive spectrometry (EDS).

### 2 Results and Discussion

Hysteresis loops of  $(\text{Sm}_{1-y}\text{Ce}_y)_2\text{Fe}_{17}\text{N}_x$  powder measured at 300 K are shown in Fig.1a. As  $y$  increases from 0 to 0.33,  $(BH)_{\text{max}}$  of  $(\text{Sm}_{1-y}\text{Ce}_y)_2\text{Fe}_{17}\text{N}_x$  powder increases slightly and then decreases. When 33 at% of Ce is substituted for Sm,  $(BH)_{\text{max}}$  changes from 141.6  $\text{kJ}/\text{m}^3$  to 140.1  $\text{kJ}/\text{m}^3$  with almost no drop (Fig.1c). The high  $(BH)_{\text{max}}$  of  $(\text{Sm}_{0.67}\text{Ce}_{0.33})_2\text{Fe}_{17}\text{N}_x$  powder originates from high  $B_r$  and high  $H_{cJ}$  of 1.1 T (Fig.1e)

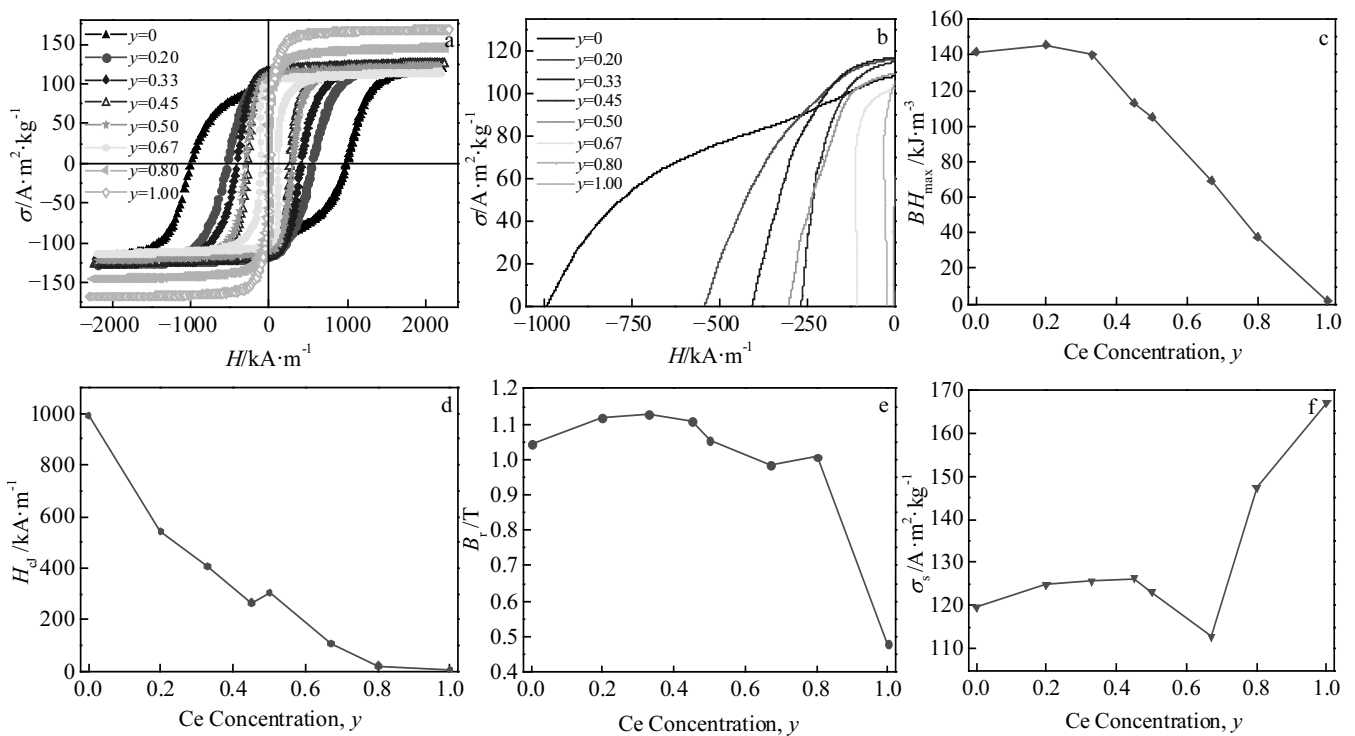


Fig.1 Magnetic measurement of  $(\text{Sm}_{1-y}\text{Ce}_y)_2\text{Fe}_{17}\text{N}_x$  powder at 300 K: (a) hysteresis loop, (b) demagnetization curves, (c) maximum energy product,  $(BH)_{\text{max}}$ , (d) intrinsic coercivity,  $H_{cJ}$ , (e) remanence,  $B_r$ , and (f) saturation magnetic polarization

and 405.8 kA/m (Fig.1d), respectively<sup>[23]</sup>. The high  $B_r$  of  $(\text{Sm}_{1-y}\text{Ce}_y)_2\text{Fe}_{17}\text{N}_x$  powder in the range of  $0 \leq y \leq 0.80$  shown in Fig.1e is derived from high  $\sigma_s$ <sup>[24]</sup>. Fig.1f shows that  $\sigma_s$  increases with increasing Ce concentration except for Ce concentrations of 0.50 and 0.67, which follows the mixing rule and is caused by the higher  $\sigma_s$  of  $\text{Ce}_2\text{Fe}_{17}\text{N}_x$  than that of  $\text{Sm}_2\text{Fe}_{17}\text{N}_x$ <sup>[24]</sup>. When the Ce concentration of  $(\text{Sm}_{1-y}\text{Ce}_y)_2\text{Fe}_{17}\text{N}_x$  powder increases from 0 to 0.33,  $\sigma_s$  of the powder increases from 119.3 A·m<sup>2</sup>/kg to 125.5 A·m<sup>2</sup>/kg. When the Ce concentration is 0.50 and 0.67, the reason for the fluctuation of  $\sigma_s$  needs further study. Fig.1d shows that  $H_{cj}$  decreases with increasing Ce concentration due to the decrease of  $H_A$ <sup>[23]</sup>. According to Ref.[16],  $H_A$  decreases with increasing Ce concentration in  $(\text{Sm}_{1-y}\text{Ce}_y)_2\text{Fe}_{17}\text{N}_x$ .

The cost of RE elements (as of October 2019<sup>[25]</sup>) in a unit mass of  $(\text{Sm}_{1-y}\text{Ce}_y)_2\text{Fe}_{17}\text{N}_x$  magnet and performance/RE price ratio of  $(\text{Sm}_{1-y}\text{Ce}_y)_2\text{Fe}_{17}\text{N}_x$  are calculated and listed in Table 1.  $(\text{Sm}_{0.67}\text{Ce}_{0.33})_2\text{Fe}_{17}\text{N}_x$  exhibits a higher performance/RE price ratio than  $\text{Sm}_2\text{Fe}_{17}\text{N}_x$ . The value increases by 39.6% when 33 at% Ce replaces Sm. The magnetic powder with 33 at% Ce substitution has excellent overall performance in terms of cost and performance. As the most abundant RE, Ce accounts for 30.2% of RE in the earth's crust, while Sm only accounts for 3.2%<sup>[14]</sup>. Replacing Sm with Ce (cheap and abundant) can solve the potential Sm shortage problem and make the utilization of RE more balanced.

The magnetization curves of  $(\text{Sm}_{1-y}\text{Ce}_y)_2\text{Fe}_{17}\text{N}_x$  powder at high temperature were examined. Uniaxial anisotropy field  $H_A$

of  $\text{Sm}_2\text{Fe}_{17}\text{N}_x$  and  $(\text{Sm}_{0.67}\text{Ce}_{0.33})_2\text{Fe}_{17}\text{N}_x$  at 100°C is shown in Fig.2 and compared with  $H_A$  at 25 °C. When the temperature is raised from 25 °C to 100 °C,  $H_A$  of  $\text{Sm}_2\text{Fe}_{17}\text{N}_x$  decreases by 32.2% from 14.9 T to 10.1 T.  $H_A$  of  $(\text{Sm}_{0.67}\text{Ce}_{0.33})_2\text{Fe}_{17}\text{N}_x$  reduces by only 15.2% from 11.2 T to 9.5 T, which is still greater than  $H_A$  of  $\text{Nd}_2\text{Fe}_{14}\text{B}$  at room temperature of 7.3 T<sup>[26]</sup>.

In order to study the effect of Ce doping on the crystal structure of  $(\text{Sm}_{1-y}\text{Ce}_y)_2\text{Fe}_{17}\text{N}_x$ , the phase composition of the nitrated powder was analyzed by XRD. Fig.3a shows the step-scanned XRD patterns (normalized) of  $(\text{Sm}_{1-y}\text{Ce}_y)_2\text{Fe}_{17}\text{N}_x$  powder. The main phase  $\text{RE}_2\text{Fe}_{17}\text{N}_x$  crystallizes in a rhombohedral  $\text{Th}_2\text{Zn}_{17}$ -type structure<sup>[21,27-30]</sup>. A schematic diagram of the crystal structure is shown in Fig.4. RE occupies a

**Table 1** Cost of RE elements in a unit mass of  $(\text{Sm}_{1-y}\text{Ce}_y)_2\text{Fe}_{17}\text{N}_x$  magnet and performance/RE price ratio of  $(\text{Sm}_{1-y}\text{Ce}_y)_2\text{Fe}_{17}\text{N}_x$

$(\text{Sm}_{1-y}\text{Ce}_y)_2\text{Fe}_{17}\text{N}_x$	$(BH)_{\max}/\text{kJ}\cdot\text{m}^{-3}$	Cost of RE elements in a unit mass of magnet/ CNY·kg <sup>-1</sup>	Performance: RE price ratio/ kJ·m <sup>-3</sup> ·CNY <sup>-1</sup> ·kg
$\text{Sm}_2\text{Fe}_{17}\text{N}_x$	141.6	69.8	2.03
$(\text{Sm}_{0.80}\text{Ce}_{0.20})_2\text{Fe}_{17}\text{N}_x$	145.6	57.5	2.53
$(\text{Sm}_{0.67}\text{Ce}_{0.33})_2\text{Fe}_{17}\text{N}_x$	140.1	49.5	2.83
$(\text{Sm}_{0.55}\text{Ce}_{0.45})_2\text{Fe}_{17}\text{N}_x$	113.0	42.0	2.69
$(\text{Sm}_{0.50}\text{Ce}_{0.50})_2\text{Fe}_{17}\text{N}_x$	105.0	38.9	2.70
$(\text{Sm}_{0.33}\text{Ce}_{0.67})_2\text{Fe}_{17}\text{N}_x$	69.2	28.3	2.45
$(\text{Sm}_{0.20}\text{Ce}_{0.80})_2\text{Fe}_{17}\text{N}_x$	37.4	20.1	1.86
$\text{Ce}_2\text{Fe}_{17}\text{N}_x$	1.6	7.5	0.21

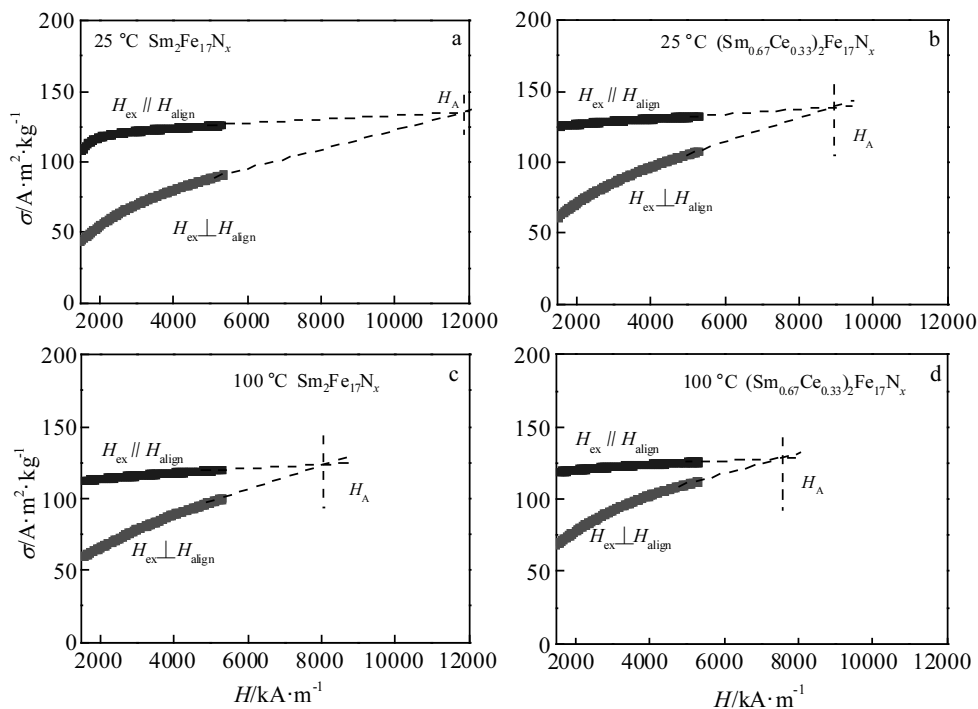


**Fig.2** First quadrant of the magnetization curves of  $\text{Sm}_2\text{Fe}_{17}\text{N}_x$  powder measured at 25 °C (a),  $(\text{Sm}_{0.67}\text{Ce}_{0.33})_2\text{Fe}_{17}\text{N}_x$  powder measured at 25 °C (b),  $\text{Sm}_2\text{Fe}_{17}\text{N}_x$  powder measured at 100 °C (c), and  $(\text{Sm}_{0.67}\text{Ce}_{0.33})_2\text{Fe}_{17}\text{N}_x$  powder measured at 100 °C (d)

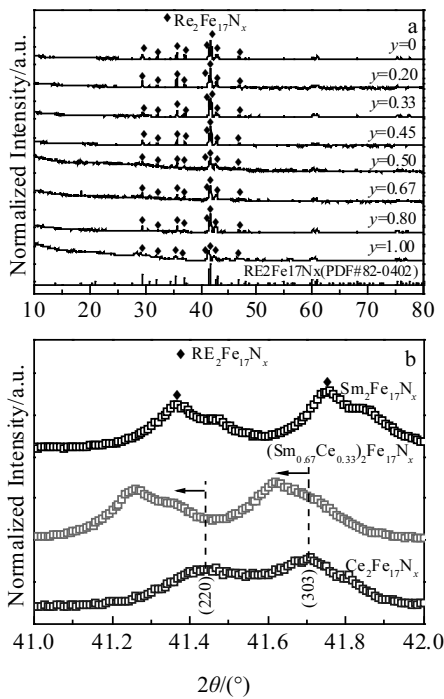


Fig.3 XRD patterns (normalized) for the powder samples of  $(\text{Sm}_{1-y}\text{Ce}_y)_2\text{Fe}_{17}\text{N}_x$  (a) and enlarged XRD patterns (normalized) of  $2\theta$  between  $41.0^\circ\sim 42.0^\circ$  for the powder samples of  $(\text{Sm}_{1-y}\text{Ce}_y)_2\text{Fe}_{17}\text{N}_x$  ( $y=0, 0.33, 1.00$ ) (b)

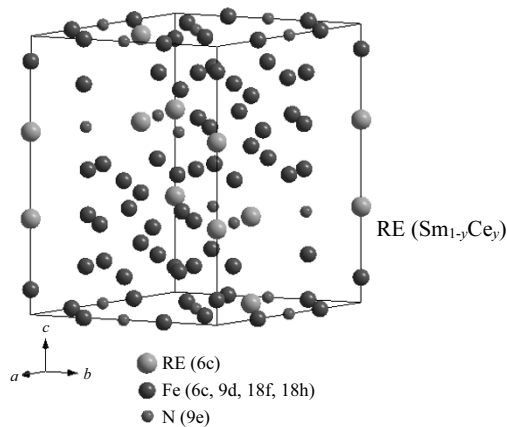


Fig.4 Crystal structure of  $\text{RE}_2\text{Fe}_{17}\text{N}_3$

unique 6c site in  $(\text{Sm}_{1-y}\text{Ce}_y)_2\text{Fe}_{17}\text{N}_x$  [29,31-34]. Different RE atoms have different radii [35]. As Ce replaces Sm, there is a possibility that the unit cell volume of  $(\text{Sm}_{1-y}\text{Ce}_y)_2\text{Fe}_{17}\text{N}_x$  changes. The change in unit-cell volume can be verified by XRD [36]. The XRD patterns (normalized) of  $(\text{Sm}_{1-y}\text{Ce}_y)_2\text{Fe}_{17}\text{N}_x$  ( $y=0, 0.33, 1.00$ ) powder amplified at  $2\theta$  from  $41.0^\circ$  to  $42.0^\circ$  are shown in Fig.3b. (303) and (220) peaks of  $(\text{Sm}_{0.67}\text{Ce}_{0.33})_2\text{Fe}_{17}\text{N}_x$  move toward a lower Bragg angle, compared with  $\text{Sm}_2\text{Fe}_{17}\text{N}_x$  and

$\text{Ce}_2\text{Fe}_{17}\text{N}_x$ . It indicates  $(\text{Sm}_{0.67}\text{Ce}_{0.33})_2\text{Fe}_{17}\text{N}_x$  has a larger unit-cell volume than  $\text{Sm}_2\text{Fe}_{17}\text{N}_x$  and  $\text{Ce}_2\text{Fe}_{17}\text{N}_x$ , due to the larger average volume of the RE site of  $(\text{Sm}_{0.67}\text{Ce}_{0.33})_2\text{Fe}_{17}\text{N}_x$ . The possible reason is the change in Ce valence. According to the speculation of Huang et al [16] and Chin et al [18], Ce is mixed valent due to the coexistence of trivalent  $4f^1$  and tetravalent  $4f^0$  electronic states in  $(\text{Sm}_{1-y}\text{Ce}_y)_2\text{Fe}_{17}\text{N}_x$ . The radius of  $\text{Ce}^{3+}$  is larger than  $\text{Ce}^{4+}$ . Ce valence shift between  $4f^1$  (+3) state and  $4f^0$  (+4) state can be verified by XPS. Surface chemical state of  $(\text{Sm}_{1-y}\text{Ce}_y)_2\text{Fe}_{17}\text{N}_x$  ( $y=0.33, 1.00$ ) was analyzed by XPS and the Ce 3d XPS spectrum is presented in Fig.5. The Ce 3d XPS spectrum exhibits 10 Gaussian-like contributions of  $\text{Ce}^{3+}$  and  $\text{Ce}^{4+}$  [37]. As listed in Table 2, peaks  $v_0, v'$  ( $\text{Ce } 3d_{5/2}$ ) and  $u_0, u'$  ( $\text{Ce } 3d_{3/2}$ ) are assigned to  $\text{Ce}^{3+}$  3d final state, while peaks  $v, v''$  ( $\text{Ce } 3d_{5/2}$ ) and  $u, u''$  ( $\text{Ce } 3d_{3/2}$ ) correspond to  $\text{Ce}^{4+}$  3d final state. Some peaks are too weak to be detected. Based on contributions in the XPS spectrum, the ratio between  $\text{Ce}^{3+}$  and  $\text{Ce}^{4+}$  can be established [38]. The ratio of  $\text{Ce}^{3+}/\text{Ce}^{4+}$  is calculated and the results are listed in Table 2. The relatively enhanced  $\text{Ce}^{3+}/\text{Ce}^{4+}$  ratio reveals the shift of Ce valence towards the  $4f^1$  (+3) state in  $(\text{Sm}_{0.67}\text{Ce}_{0.33})_2\text{Fe}_{17}\text{N}_x$ . The  $\text{Ce}^{3+}$  configuration with one localized 4f moment is beneficial for enhancing magneto-crystalline anisotropy and net magnetic moment. Thus reduction of  $(BH)_{\text{max}}$  and  $H_{c1}$  in  $(\text{Sm}_{0.67}\text{Ce}_{0.33})_2\text{Fe}_{17}\text{N}_x$  is suppressed. The reason for the shift of Ce valence is presumed to be an increase in the degree of component confusion.

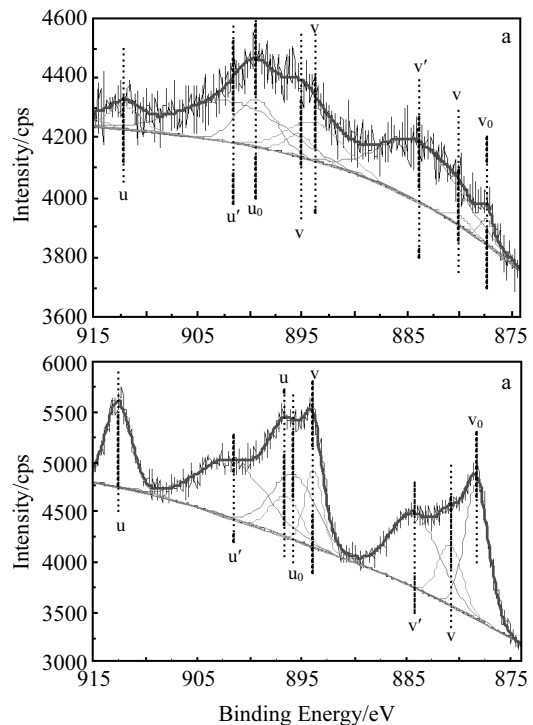


Fig.5 XPS spectra of Ce 3d of  $(\text{Sm}_{0.67}\text{Ce}_{0.33})_2\text{Fe}_{17}\text{N}_x$  (a) and  $\text{Ce}_2\text{Fe}_{17}\text{N}_x$  (b)

**Table 2** Ratio of Ce<sup>3+</sup>/Ce<sup>4+</sup>

Peak assignment	Ce contribution	Electronic states	(Sm <sub>0.67</sub> Ce <sub>0.33</sub> ) <sub>2</sub> Fe <sub>17</sub> N <sub>x</sub>		Ce <sub>2</sub> Fe <sub>17</sub> N <sub>x</sub>	
			Peak	Area	Peak	Area
v <sub>0</sub>	Ce <sup>3+</sup>	Trivalent 4f <sup>1</sup>	877.31	135.24	878.24	3 980.67
v	Ce <sup>4+</sup>	Tetravalent 4f <sup>0</sup>	879.94	95.47	880.80	1 747.40
v'	Ce <sup>3+</sup>	Trivalent 4f <sup>1</sup>	883.79	1 882.37	884.13	4 318.79
v''	Ce <sup>4+</sup>	Tetravalent 4f <sup>0</sup>	893.74	877.21	Not detected	None
v'''	Ce <sup>4+</sup>	Tetravalent 4f <sup>0</sup>	895.19	264.79	893.85	1 663.35
u <sub>0</sub>	Ce <sup>3+</sup>	Trivalent 4f <sup>1</sup>	899.43	760.35	895.77	3 615.96
u	Ce <sup>4+</sup>	Tetravalent 4f <sup>0</sup>	Not detected	none	896.54	1 488.73
u'	Ce <sup>3+</sup>	Trivalent 4f <sup>1</sup>	901.71	1 670.70	901.61	4 698.64
u''	Ce <sup>4+</sup>	Tetravalent 4f <sup>0</sup>	Not detected	None	Not detected	None
u'''	Ce <sup>4+</sup>	Tetravalent 4f <sup>0</sup>	912.11	317.79	912.55	2 661.58
Total			6 003.92		24 175.12	
Ce <sup>3+</sup>			4 448.66		16 614.06	
Ce <sup>4+</sup>			1 555.26		7 561.06	
Ce <sup>3+</sup> /Ce <sup>4+</sup> (trivalent 4f <sup>1</sup> /tetravalent 4f <sup>0</sup> )			2.86		2.20	

(Sm<sub>1-y</sub>Ce<sub>y</sub>)<sub>2</sub>Fe<sub>17</sub>N<sub>x</sub> has a high  $H_{cJ}$  and cannot be characterized by ordinary electron microscopy. Considering the inheritance of the alloy structure, the unnitrided (Sm<sub>1-y</sub>Ce<sub>y</sub>)<sub>2</sub>Fe<sub>17</sub> alloy was analyzed by SEM to obtain the distribution of Ce in (Sm<sub>1-y</sub>Ce<sub>y</sub>)<sub>2</sub>Fe<sub>17</sub>N<sub>x</sub>. Fig.6a and 6b give SEM-BSE images of cross-section of the annealed (Sm<sub>1-y</sub>Ce<sub>y</sub>)<sub>2</sub>Fe<sub>17</sub> (y=0.33, 0.50) alloys. The bright regions are phases rich in RE elements. The grey regions are related to the RE<sub>2</sub>Fe<sub>17</sub> matrix phase. In order to fully understand the microstructure and chemical composition, the element composition of bright and grey regions was characterized by EDS. Although the EDS results show a slight composition shift as a

semi-quantitative analysis, they can be used to assist in determining the phase. The atomic percentages of the Fe, Ce, and Sm elements of the spots in Fig.6a and 6b are listed in Table 3. According to the atomic ratio of Fe/(Sm+Ce), the bright region in the annealed (Sm<sub>0.67</sub>Ce<sub>0.33</sub>)<sub>2</sub>Fe<sub>17</sub> alloy is evaluated as the REFe<sub>3</sub> phase. The bright areas in the annealed (Sm<sub>0.5</sub>Ce<sub>0.5</sub>)<sub>2</sub>Fe<sub>17</sub> alloy are evaluated as the REFe<sub>2</sub> phase. The difference in phase composition may be related to the nominal composition of (Sm<sub>1-y</sub>Ce<sub>y</sub>)<sub>2</sub>Fe<sub>17</sub> alloy and requires further investigation. Since the phase volume of the REFe<sub>2</sub>/REFe<sub>3</sub> phase is relatively low, it is not detected in the XRD pattern of the (Sm<sub>1-y</sub>Y<sub>y</sub>)<sub>2</sub>Fe<sub>17</sub>N<sub>x</sub> powder. As listed in Table 3, the atomic

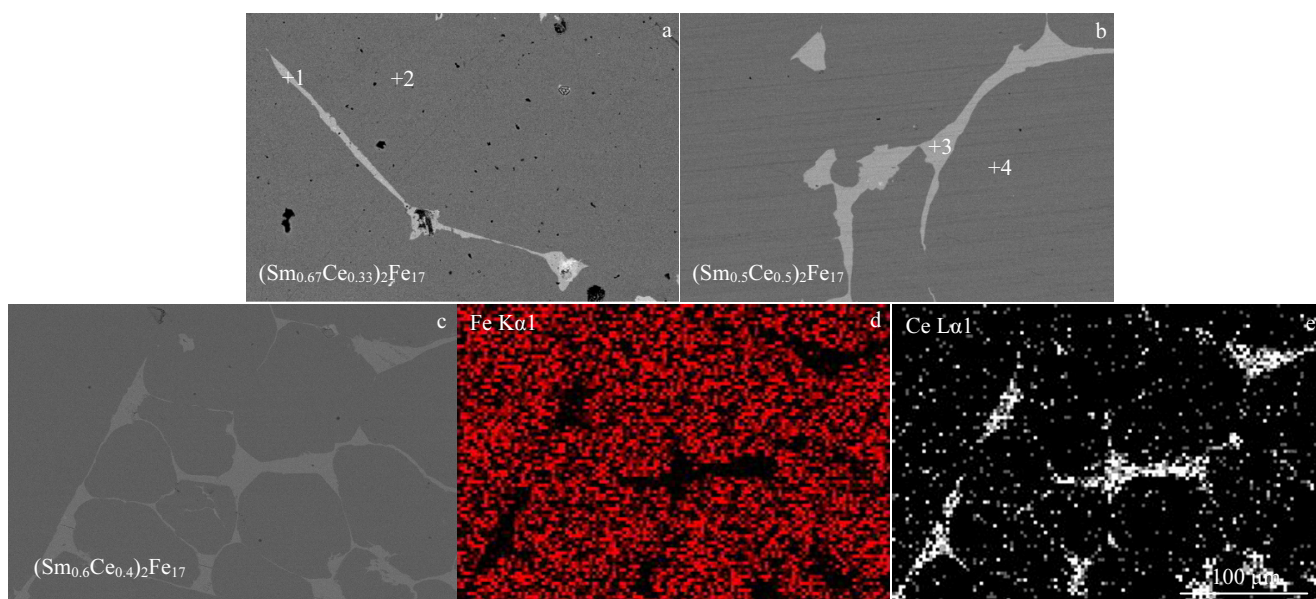


Fig.6 SEM-BSE images of cross-section of annealed (Sm<sub>0.67</sub>Ce<sub>0.33</sub>)<sub>2</sub>Fe<sub>17</sub> (a), (Sm<sub>0.5</sub>Ce<sub>0.5</sub>)<sub>2</sub>Fe<sub>17</sub> (b) and (Sm<sub>0.6</sub>Ce<sub>0.4</sub>)<sub>2</sub>Fe<sub>17</sub> (c); elemental mappings of Fe Kα1 (d) and Ce Lα1 (e) for annealed (Sm<sub>0.6</sub>Ce<sub>0.4</sub>)<sub>2</sub>Fe<sub>17</sub>

**Table 3 Atomic percentages of Fe, Ce, and Sm for spots 1, 2, 3 and 4 in Fig.6a, 6b and atomic ratio of Fe/(Sm+Ce) and Ce/Sm**

Fig.6a	Spot 1	Spot 2
Fe	74.17	88.93
Ce	11.25	2.16
Sm	14.58	8.91
Atomic ratio of Fe/(Sm+Ce)	2.87	8.03
Atomic ratio of Ce/Sm	0.78	0.24
Fig.6b	Spot 3	Spot 4
Fe	65.47	88.73
Ce	18.76	3.55
Sm	15.77	7.72
Atomic ratio of Fe/(Sm+Ce)	1.90	7.87
Atomic ratio of Ce/Sm	1.19	0.46

ratio of Ce/Sm in the bright region is higher than that in the grey regions, which means that Ce tends to diffuse into the REFe<sub>3</sub>/REFe<sub>2</sub> phase rather than the RE<sub>2</sub>Fe<sub>17</sub> phase. The Fe Kα1 and Ce La1 mappings in Fig.6d and 6e also reflect the segregation behavior of Ce at the grain boundaries. Since the microstructure of (Sm<sub>1-y</sub>Ce<sub>y</sub>)<sub>2</sub>Fe<sub>17</sub>N<sub>x</sub> powder inherits from the microstructure of the annealed (Sm<sub>1-y</sub>Ce<sub>y</sub>)<sub>2</sub>Fe<sub>17</sub> alloy, this aggregation behavior can reduce the true Ce content of RE<sub>2</sub>Fe<sub>17</sub>N<sub>x</sub> main phase and help increasing H<sub>cj</sub> of the nitrides. The thermodynamic origin of Ce segregation in annealed (Sm<sub>1-y</sub>Ce<sub>y</sub>)<sub>2</sub>Fe<sub>17</sub> alloy may be related to the substitution energy of Ce in the RE<sub>2</sub>Fe<sub>17</sub> phase, which requires first-principles density functional calculation.

### 3 Conclusions

1) When 33 at% of Ce is substituted for Sm, maximum energy product (BH)<sub>max</sub> of (Sm<sub>1-y</sub>Ce<sub>y</sub>)<sub>2</sub>Fe<sub>17</sub>N<sub>x</sub> changes from 141.6 kJ/m<sup>3</sup> to 140.1 kJ/m<sup>3</sup> with almost no decrease. Accordingly, performance/rare earth (RE) price ratio increases by 39.6%.

2) The relatively high intrinsic coercivity H<sub>cj</sub> of 405.8 kA/m and undiminished remanence B<sub>r</sub> of 1.1 T result in a high (BH)<sub>max</sub> of (Sm<sub>0.67</sub>Ce<sub>0.33</sub>)<sub>2</sub>Fe<sub>17</sub>N<sub>x</sub>.

3) For (Sm<sub>1-y</sub>Ce<sub>y</sub>)<sub>2</sub>Fe<sub>17</sub>N<sub>x</sub>, B<sub>r</sub> maintains a large value in the range of 0 ≤ y ≤ 0.80. As the Ce content increases, H<sub>cj</sub> of (Sm<sub>1-y</sub>Ce<sub>y</sub>)<sub>2</sub>Fe<sub>17</sub>N<sub>x</sub> decreases.

4) At 100 °C, anisotropy field (H<sub>A</sub>) of (Sm<sub>0.67</sub>Ce<sub>0.33</sub>)<sub>2</sub>Fe<sub>17</sub>N<sub>x</sub> is 9.5 T, which is still greater than H<sub>A</sub> of Nd<sub>2</sub>Fe<sub>14</sub>B at room temperature.

5) Ce tends to diffuse into the REFe<sub>3</sub>/REFe<sub>2</sub> phase rather than the RE<sub>2</sub>Fe<sub>17</sub> matrix phase. This aggregation behavior reduces the true Ce content of the main phase RE<sub>2</sub>Fe<sub>17</sub>N<sub>x</sub> and increases H<sub>cj</sub> of the nitrides. Ce valence shifts towards the moment-carrying 4f<sup>1</sup> (+3) state in (Sm<sub>0.67</sub>Ce<sub>0.33</sub>)<sub>2</sub>Fe<sub>17</sub>N<sub>x</sub>, which contributes to the enhancement of magnetocrystalline anisotropy and net magnetic moment.

### References

- 1 Tsunata R, Takemoto M, Ogasawara S et al. 2016 XXII International Conference on Electrical Machines (ICEM)[C]. New York: IEEE, 2016: 272
- 2 Yu F, Takemoto M, Ogasawara S et al. 2017 IEEE International Electric Machines and Drives Conference (IEMDC)[C]. Piscataway: IEEE, 2017: 8
- 3 Coey J M D, Sun H. *Journal of Magnetism and Magnetic Materials*[J], 1990, 87(3): 251
- 4 Xu J W, Zheng J W, Chen H B et al. *Journal of Rare Earths*[J], 1990, 37(6): 638
- 5 Chen H B, Zheng J W, Qiao L et al. *Rare Metals*[J], 2018, 37(11): 989
- 6 Chen H B, Xu J W, Zheng J W et al. *Science of Advanced Materials*[J], 2016, 8(10): 1978
- 7 Xiao X F, Si P Z, Ge H L et al. *Journal of Electronic Materials*[J], 2018, 47(12): 7472
- 8 Hosokawa A, Takagi K. *Acta Materialia*[J], 2017, 136: 366
- 9 Diop L V B, Kuz'min M D, Skokov K P et al. *Physical Review B*[J], 2016, 94(14): 8
- 10 Buschow K H J. *Reports on Progress in Physics*[J], 1991, 54(9): 1123
- 11 Schnitzke K, Schultz L, Wecker J et al. *Applied Physics Letters*[J], 1990, 57(26): 2853
- 12 Sun A, Tong C, Su G et al. *Journal of Magnetic Materials and Devices*[J], 2005, 36(6): 7 (in Chinese)
- 13 Yang J, Han J, Liu S et al. *Materials China*[J], 2015, 34(11): 819 (in Chinese)
- 14 Dong S Z, Li W, Chen H S et al. *AIP Advances*[J], 2017, 7(5): 6
- 15 Fa B. *The 6th China Baotou Rare Earth Industry BBS, Rare Earth Information*[C]. Baotou: National Engineering Research Centre of Rare Earth Metallurgy, 2014: 4 (in Chinese)
- 16 Huang M Q, Zheng Y, Miller K et al. *Journal of Magnetism and Magnetic Materials*[J], 1991, 102(1-2): 91
- 17 Pandey T, Du M H, Parker D S et al. *Physical Review Applied*[J], 2018, 9(3): 13
- 18 Chin T S, Cheng K H, Yao J M. *Journal of Alloys and Compounds*[J], 1995, 222: 148
- 19 Christodoulou C N, Takeshita T. *Journal of Alloys and Compounds*[J], 1993, 194(1): 113
- 20 Okada S, Suzuki K, Node E et al. *Journal of Alloys and Compounds*[J], 2017, 695: 1617
- 21 Iriyama T, Kobayashi K, Imaoka N et al. *IEEE Transactions on Magnetics*[J], 1992, 28(5): 2326
- 22 Matsuura M, Yarimizu K, Osawa Y et al. *Journal of Magnetism and Magnetic Materials*[J], 2019, 471: 310
- 23 Hu B P, Rao X L, Wang Y Z. *Rare-Earth Permanent Magnet*[M]. Beijing: Metallurgical Industry Press, 2017: 227 (in Chinese)
- 24 Zhou S Z, Dong Q F. *Super Permanent Magnet*[M]. Beijing: Metallurgical Industry Press, 2004: 51, 55, 129, 402, 414 (in Chinese)
- 25 Shanghai Metals Market, Pricing of Rare Earth Metals. Available

- at: <https://price.metal.com/prices/rare-earth/rare-earth-metals>, 2019
- 26 Niu E, Chen Z A, Chen G A et al. *Journal of Applied Physics*[J], 2014, 115(11): 14
- 27 Sun H, Coey J M D, Otani Y et al. *Journal of Physics-Condensed Matter*[J], 1990, 2(30): 6465
- 28 Franse J J M, Radwański R J. *Handbook of Magnetic Materials*[M]. Amsterdam: Elsevier, 1993: 307
- 29 Inami N, Takeichi Y, Ueno T et al. *Journal of Applied Physics*[J], 2014, 115(17): 3
- 30 Itoh M, Machida K, Nakajima H et al. *Journal of Alloys and Compounds*[J], 1999, 288(1-2): 141
- 31 Coey J M D, Smith P A I. *Journal of Magnetism and Magnetic Materials*[J], 1999, 200(1-3): 405
- 32 Alonso P A, Gorria P, Cuello G et al. In: Velasco J H, Garcia C C, Castellote M Eds. *6th Meeting of the Spanish Neutron Scattering Association*[C]. Bristol: Iop Publishing Ltd, 2014
- 33 Yang C J, Lee W Y, Shin H S. *Journal of Applied Physics*[J], 1993, 74(11): 6824
- 34 Coey J M D. *Physica Scripta*[J], 1991, T39: 21
- 35 Hu Y. In: Li M, Liu Z, Wu J, Hu Y Eds. *Rare Earth Elements and Their Analytical Chemistry*[M]. Beijing: Chemical Industry Press, 2009: 30 (in Chinese)
- 36 Ye J W, Ying L, Dong W et al. *Rare Metal Materials and Engineering*[J], 2006, 35(11): 1835 (in Chinese)
- 37 Tang D D, Zhang G K. *Chemical Engineering Journal*[J], 2016, 283: 721
- 38 Wang A Q, Panchaipetch P, Wallace R M et al. *Journal of Vacuum Science & Technology B*[J], 2003, 21(3): 1169

## Ce 掺杂对 $(\text{Sm}_{1-y}\text{Ce}_y)_2\text{Fe}_{17}\text{N}_x$ 结构和磁性能的影响

徐健伟<sup>1</sup>, 郑精武<sup>1</sup>, 陈海波<sup>2</sup>, 乔梁<sup>1</sup>, 应耀<sup>1</sup>, 蔡伟<sup>1</sup>, 李旺昌<sup>1</sup>, 余靓<sup>1</sup>, 林旻<sup>3</sup>, 车声雷<sup>1</sup>

(1. 浙江工业大学, 浙江 杭州 310014)

(2. 杭州海声科技有限公司, 浙江 杭州 310019)

(3. 中国科学院宁波材料技术与工程研究所, 浙江 宁波 315201)

**摘要:** 研究了完全氮化的 $(\text{Sm}_{1-y}\text{Ce}_y)_2\text{Fe}_{17}\text{N}_x$  ( $y=0, 0.20, 0.33, 0.45, 0.50, 0.67, 0.80, 1.00$ ) 粉末的磁性能和微观结构。当用 33at% Ce 代替 Sm 时, 最大磁能积 $(BH)_{\max}$  从  $141.6 \text{ kJ/m}^3$  变为  $140.1 \text{ kJ/m}^3$ , 几乎没有下降。相应地, 性能/稀土价格比率提高了 39.6%。根据能量色散光谱 (EDS) 分析, Ce 倾向于分布在  $\text{REFe}_3/\text{REFe}_2$  晶界相中。XPS 证实了 $(\text{Sm}_{1-y}\text{Ce}_y)_2\text{Fe}_{17}\text{N}_x$  中 Ce 离子的价态变化。

**关键词:**  $\text{Sm}_2\text{Fe}_{17}\text{N}_x$ ; Ce 取代; 最大磁能积; 相偏聚; Ce 变价

作者简介: 徐健伟, 男, 1992 年生, 博士, 浙江工业大学材料科学与工程学院, 浙江 杭州 310014, 电话: 0571-88871530, E-mail: 596976371@qq.com